



Microfluidics-guided fluorescent nanodiamond assembly method for highly sensitive thermometry

Keita Saikawa^a, Masaya Zetsu^a, Daiki Ueshima^a, Taiichi Shikama^a, Ken-ichiro Kamei^{b,c,d,e,f,g}, Osamu Tabata^h, Yoshikazu Hirai^{a,*} 

^a Department of Mechanical Engineering and Science, Kyoto University, Kyoto Daigaku Katsura, Nishikyo-ku, Kyoto 615-8540, Japan

^b Program of Biology, Division of Science, New York University Abu Dhabi, Abu Dhabi, UAE

^c Program of Bioengineering, Division of Engineering, New York University Abu Dhabi, Abu Dhabi, UAE

^d Department of Biomedical Engineering, Tandon School of Engineering, New York University, Brooklyn, NY 11201, USA

^e Institute for Integrated Cell-Material Sciences (WPI-iCeMS), Institute for Advanced Study, Kyoto University, Yoshida-Ushinomiya-cho, Sakyo-ku, Kyoto 606-8501, Japan

^f Department of Pharmaceutics, Wuyi College of Innovation, Shenyang Pharmaceutical University, Shenyang, Liaoning 110016, PR China

^g Department of Pharmaceutics, School of Pharmacy, Shenyang Pharmaceutical University, Shenyang, Liaoning 110016, PR China

^h Faculty of Engineering/Graduate School of Engineering, Kyoto University of Advanced Science, Gotanda-cho, Yamanouchi, Ukyo-ku, Kyoto 615-8577, Japan

ARTICLE INFO

Keywords:

Fluorescent nanodiamonds
Nitrogen-vacancy centers
Thermometry
Particle assembly
Microfluidics
Quantum sensing

ABSTRACT

Fluorescent nanodiamonds (FNDs) with nitrogen vacancy centers (NVCs) show promise for use as thermometers owing to their unique physicochemical and optical properties. FND-based thermometry has been steadily developing and is now transitioning into the practical application phase. Various approaches have been proposed for FND assembly, which is a key process for temperature mapping applications. However, the assembly of high-sensitivity FND thermometers remains challenging because it requires the fabrication of three-dimensionally aggregated FNDs across the target area to generate a strong fluorescence signal. To overcome this drawback, we aimed to enable the microfluidics-guided assembly of FNDs to enhance the sensitivity of FND-based thermometry. Specifically, a microfluidic template with through-holes was used to fabricate vertically aggregated FNDs (FND clusters) on a substrate, thereby improving the signal-to-noise ratio (SNR) by superimposing the individual fluorescence events of the FNDs. The FND clusters were arrayed over a millimeter-scale area, and sensitivity improvements were achieved through vertical aggregation. Furthermore, the fluorescence spectra of the FND clusters were investigated to test the increase in temperature-mapping accuracy. Our microfluidics-guided assembly method has potential as a practical approach for creating an array of high-sensitivity FND thermometers on scalable substrates, broadening their use in various fields such as chemistry, electronics, and biology.

1. Introduction

Fluorescent nanodiamonds (FNDs) containing nitrogen vacancy centers (NVCs) have been used as quantum sensors in various fields such as chemistry, electronics, and biology[1–3]. FND quantum sensors leverage the changes in the spin-state and ground-excited energy levels of NVCs, which manifest as fluorescence, in response to external environments including magnetic fields[4], electric fields[5], temperature [6,7], and pH[8]. Among them, FND thermometers have gained significant attention owing to their high thermal conductivity (2000 W/K·m),

which enables rapid thermal responses[9]. The physicochemical inertness and photobleaching/photoblinking-free[10] fluorescence of NVCs permit reliable and continuous temperature measurements, offering a significant advantage over other non-contact fluorescence-based methods using organic dyes or fluorescent proteins[3,7,11]. Furthermore, FNDs have a wide operating temperature range (100–700 K)[12] suitable for cryogenics[13] and microelectronics[14,15]. FNDs also exhibit biocompatibility[16,17], and are amenable to surface modification for binding with molecules or materials[18]. A high signal-to-noise ratio (SNR) is required to achieve sensitive thermometry

* Corresponding author.

E-mail addresses: saikawa.keita.3p@kyoto-u.ac.jp (K. Saikawa), ztsh122000@gmail.com (M. Zetsu), ueshima.daiki.83x@st.kyoto-u.ac.jp (D. Ueshima), shikama.taiichi.7w@kyoto-u.ac.jp (T. Shikama), kk4801@nyu.edu (K.-i. Kamei), tabata.osamu@kuas.ac.jp (O. Tabata), hirai@me.kyoto-u.ac.jp (Y. Hirai).

<https://doi.org/10.1016/j.sna.2025.116312>

Received 3 December 2024; Received in revised form 27 January 2025; Accepted 11 February 2025

Available online 12 February 2025

0924-4247/© 2025 The Author(s). Published by Elsevier B.V. This is an open access article under the CC BY license (<http://creativecommons.org/licenses/by/4.0/>).

using FNDs. Thus, for achieving high fluorescence intensities, exciting an ensemble of FNDs and superimposing their individual fluorescence events is an effective approach^{14,19}. In particular, aggregated FNDs function as high-sensitivity thermometers because the fluorescence intensity depends on the number of simultaneously excited FNDs. Therefore, techniques for assembling aggregated FNDs on target sites or substrates are crucial^[14,15,19,20], to realize practical applications such as temperature mapping for noncontact heat transfer analysis and detecting localized heating.

Various FND assembly methods have been proposed to satisfy the aforementioned requirements. Optical tweezers can capture FNDs and aggregate them, forming three-dimensional (3D) microspheres; however, a specialized optical system^[19] is required, and their scalability for temperature mapping applications across multiple measurement points is limited by the need to individually manipulate the microspheres. Functional groups or metal patterns on target substrates, used as templates, can serve as alternative approaches for directly assembling the FNDs on the substrate^[15,21–23]. However, the FND-substrate interactions typically result in monolayer-like assemblies, leading to a lower fluorescence intensity than that of 3D aggregates. Therefore, a practical method must be devised to collectively and vertically aggregate FNDs on target substrates to effectively enhance the sensitivity by assembling FNDs within defined spots of a specific size excited by a laser.

In this study, a microfluidics-guided assembly method was devised to allow the fabrication of vertically aggregated FND clusters on the target substrate to enhance the SNR and sensitivity. A polydimethylsiloxane (PDMS)-based microfluidic structure fabricated by multilayered soft lithography was used as a microfluidic template, which contained through-holes for vertically and directly aggregating the FNDs onto the target substrate at multiple positions. The fluorescence intensity of each cluster was investigated, and the vertically aggregated FNDs were found to exhibit significantly enhanced SNR. The temperature sensitivity of the clusters was explored to prove that enhancing the SNR increased the sensitivity. Furthermore, the fluorescence spectrum of the FND clusters was analyzed, and the vertical aggregation of FNDs was found to exhibit improved accuracy for temperature mapping.

2. Microfluidics-guided assembly

A microfluidics-guided assembly method was used to vertically

aggregate the FNDs on the target substrate (Fig. 1(a)). The microfluidic template featured an array of through-holes connected by another channel (Fig. 1(b)), enabling the vertical, collective, and direct aggregation of FNDs within the spots defined by the template on the substrate (see Fig. 1(c) for an illustration of the assembly process). First, the microfluidic template was placed on the target substrate, and the through-holes were sealed against the substrate. This sealing can be achievable on various flat substrates due to the conformability and elasticity of PDMS, which allows it to closely adapt and adhere to the surface. To fill the through-holes with the FND suspension, the microfluidic template and substrate were maintained under vacuum in a desiccator before the FND suspension was injected^[24,25]. Owing to the gas permeability of PDMS, gas was removed from the PDMS and channel during this degassing step. Subsequently, the FND suspension was injected into the inlet. The evacuated PDMS absorbed the gas remaining in the through-holes, and the suspension was drawn into the through-holes. The FNDs aggregated on the substrate as the suspension dried, forming FND clusters after the suspension completely evaporated. Finally, the template was removed from the substrate, leaving behind FND clusters on the substrate.

3. Materials and methods

3.1. Fabrication of PDMS microfluidic template

The PDMS-based microfluidic template comprised two layers: a patterned layer and a channel layer. The patterned layer had an array of through-holes, and the channel layer contained a conduit to introduce the FND suspension. The template was fabricated using gas-permeable PDMS (Dow Corning, SYLGARD 184, U.S.) (see Fig. 2 for its fabrication process).

The mold for the channel layer was prepared using a 3D printer (Formlabs, Form3, U.S.) with a resin (Formlabs, Durable Resin, U.S.). The 150- μm -tall mold was cleaned after printing. The PDMS base and curing agent were mixed at a weight ratio of 10:1, and the mixture was poured into the mold and cured at 75 °C for at least 2 h. After peeling off the PDMS structure from the mold, inlet and outlet ports were created using a biopsy punch.

The mold for the patterned layer was fabricated on a 4-inch silicon wafer by UV lithography. A 40- μm -thick negative photoresist (TOKYO OHKA KOGYO, TMMR S2000™, Japan) was first patterned using a

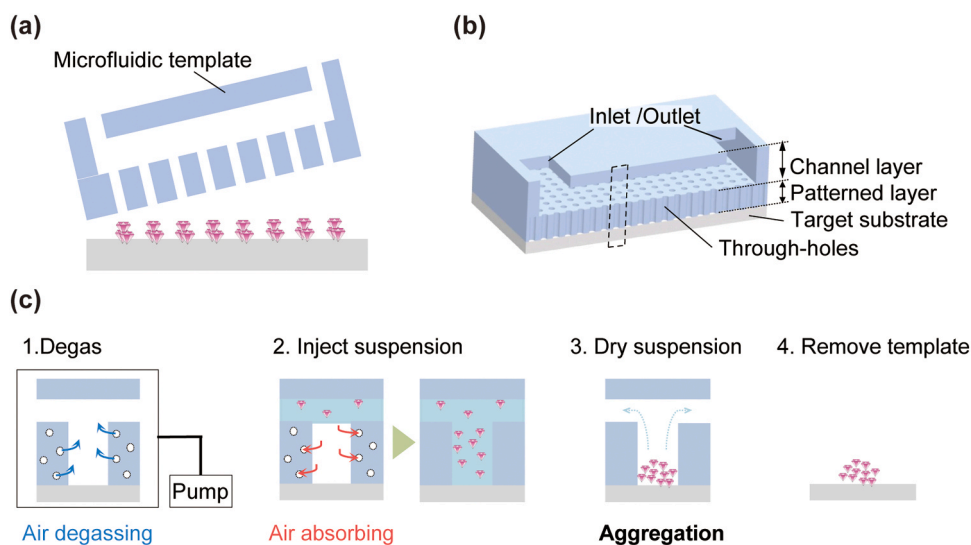


Fig. 1. Microfluidics-guided assembly of fluorescence nanodiamonds (FNDs). **a** Illustration of the microfluidics-guided FND assembly method. **b** Structure of microfluidic template configured for the devised assembly method. The patterned layer has arrayed through-holes, and the FND suspension is supplied through the inlet and channel layer. **c** Process flow of FND assembly. After the template makes contact with the substrate, the PDMS structure is degassed. Subsequently, the FND suspension is injected from the inlet. The template is removed from the substrate after the suspension dries.

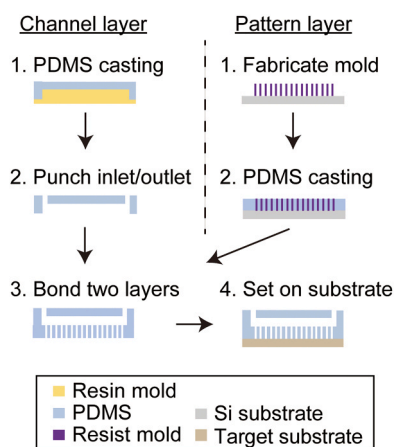


Fig. 2. Schematic illustrating fabrication of the microfluidic template.

standard photolithography tool. UV exposure was performed using a mask aligner (Japan Science Engineering Co. Ltd., MUM-1000 Series, Japan)[26,27]. After hard baking the mold at 200 °C for an hour, a release agent (Shin-Etsu Silicones, Barrier coat No.7, Japan) was spin-coated to facilitate the removal of PDMS from the mold. The PDMS base and curing agent were mixed at a curing ratio of 10:1, and the mixture was spin-coated over the mold and cured at 80 °C for at least 30 min. To create through-holes, the PDMS on top of the mold was etched with O₂/CF₄ plasma using a plasma etcher (Samco, FA-1, Japan). To prevent rupture of the patterned layer when it was peeled off the Si substrate, a supporting layer (AICELLO, SO sheet, Japan) was bonded to the PDMS patterned layer using vacuum ultraviolet (VUV) radiation and then heated at 75 °C for at least 6 h to achieve robust bonding. The supporting layer contained a water-soluble polyvinyl alcohol (PVA) layer on a polyethylene terephthalate (PET) layer. The PDMS patterned layer was peeled off along with the supporting layer and then bonded to the bottom of the channel layer using VUV radiation to form the microfluidic template. Subsequently, the template was immersed in water (80 °C) to remove the supporting layer, and O₂ plasma ashing was conducted using the plasma etcher to remove the residue of the supporting layer from the surface of the template.

3.2. Microfluidics-guided assembly

The target substrate for assembling FNDs was prepared by spin-coating PDMS onto a glass substrate. The PDMS base and curing agent were mixed at a weight ratio of 10:1. The patterned layer of the template was attached to the substrate, and the through-holes were sealed against the substrate. The template and substrate were then degassed for at least 1 h in a desiccator to remove the gas inside the template[25]. Within 1 min of extricating the template from the desiccator, a 5 µL FND suspension was introduced from the inlet of the template. The FND suspension was then dried at 30 °C for over 12 h in an oven to aggregate FNDs on the substrate. Finally, the microfluidic template was peeled off from the substrate. The assembly was also applied to other substrate materials including Si, glass, Al₂O₃, and a collagen vitrigel membrane (Kanto Chemical Co., Japan) using the same protocol.

3.3. Fluorescent nanodiamonds

Three different commercially available FND suspensions with the following average FND diameters were used: 70 nm (Adamas Nanotechnology, NDNV70nmHi10mL, ~3 ppm NV, 0.1 % w/v, U.S.), 140 nm (Adamas Nanotechnology, NDNV140nmHi10mL, ~3 ppm NV, 0.1 % w/v, U.S.), and 750 nm (Adamas Nanotechnology, MDNV1µmHi10mg, ~3.5 ppm NV, 0.1 % w/v, U.S.). Prior to being injected into the template, the 70 nm and 140 nm FND suspensions were concentrated to 1.0,

2.0, and 4.0 % w/v, whereas the 750 nm FND suspension was concentrated to 0.25, 0.50, and 1.0 % w/v.

3.4. Field-emission scanning electron microscopy

The FND clusters were examined by field-emission scanning electron microscopy (FE-SEM, Hitachi High-Tech, SU-8020, Japan). Prior to this analysis, the samples were coated with a thin layer of platinum-palladium using a sputter coater (Hitachi, E-1030, Japan).

3.5. Laser scanning microscopy

Height profiles of the FND clusters were acquired by laser scanning microscopy (KEYENCE, VK-X3000, Japan) at 150 × magnification. The obtained height profiles were postprocessed using the Keyence software function for leveling onto the substrate. The volume of each cluster was estimated from the height data.

3.6. Fluorescence measurement

To investigate the fluorescence intensity and temperature-measurement performance of the FND clusters, the fluorescence spectrum of each cluster was acquired using a custom-made scanning epifluorescence microscope. The temperature-measurement performance of the FND clusters was evaluated using all-optical methods[7,28]. All-optical methods can perform temperature measurements using a simple optical system compared with that of spin-based methods, which require both optical and magnetic excitation to control the spin state of NVCs[7]. In all-optical methods, the temperature is derived from the ZPL of the NVCs; the ZPL peak wavelength was used as an indicator of temperature in the present study. To excite the NVCs, a 594-nm laser (Cobolt, Mambo, Sweden) was focused onto the FND clusters using an objective lens (Sigma-Koki, EPLE-20, 20x, Japan) with an adjusted spot diameter of ~20 µm and intensity of 0.5 mW. The laser-irradiated position on the sample substrate was set using a three-axis motorized stage (Suruga Seiki, KXC-06020-C, 2 µm resolution, 0.2 µm repeatability, Japan). The fluorescence from each FND cluster was captured using the same objective lens, following which spectra in the 605–740 nm range were acquired using a spectrometer (85 mm focal length, 300 lines/mm grating, F/1.8) equipped with a CMOS camera (Basler, acA1920-155um, 1920 × 1200 pixels, 5.86 µm squared pixel size, Germany) after wavelength filtering with a dichroic mirror (Thorlabs, DMLP605, 605 nm cut-on) and a notch filter (Thorlabs, NF594-23, 594 nm central wavelength, 23 nm full width at half maximum (FWHM), U.S.). Prior to spectral analysis, the relative intensity and absolute wavelength of the acquired spectra were calibrated using a standard tungsten halogen lamp and helium atomic emission lines of known wavelengths from an AC glow discharge tube, respectively. In this system, the wavelength resolution was 1.5 nm at the FWHM, and the reciprocal linear dispersion was 0.23 nm/pixel at 638 nm.

The FND clusters were placed on a temperature-regulated stage to investigate the temperature dependence of their ZPL. The surface temperature of the plate was measured using a Pt100 sensor (RS Pro, Class A, U.K.) and digitizer (National Instruments NI9217, 24-bit, 400 S/s, U.S.), with the current fed to the Peltier element subjected to PID control to maintain a constant stage temperature. The spatial uniformity of temperature over the sample area and its temporal stability were within 0.1 K.

3.7. Fluorescence spectrum analysis

To determine the ZPL peak wavelength and the FWHM of the ZPL as indicators of temperature and spectral sharpness, respectively, the fluorescence spectra of the FND clusters were analyzed using Python (ver 3.9.7). Least-squares fitting was conducted for each spectrum using the scipy.optimize module (ver 1.7.1). The fitting function $f(\lambda)$ was the

sum of the Voigt and exponential functions representing the ZPL (Lorentzian function) convolved with the instrument function (Gaussian function) and phonon side band spectra, respectively [28], as follows:

$$f(\lambda) = \int_{-\infty}^{\infty} B \exp\left(-4 \ln_2 \frac{\tau^2}{W_G^2}\right) \frac{A}{\pi} \frac{W_L}{4\{(\lambda - \tau) - \lambda_0\}^2 + W_L^2} d\tau + I_0 \exp(b\lambda), \quad (1)$$

where W_G is the width of the spectrometer instrument; A is the ZPL area; W_L is the ZPL FWHM; λ_0 is the ZPL peak wavelength; and B , I_0 , and b are constants. The fluorescence intensity was calculated as the sum of the intensities in the range of 620–760 nm, where the fluorescence of NVCs was observed.

4. Results

4.1. Fabrication of the PDMS microfluidic template

The microfluidic template comprised a patterned layer and a channel layer. The patterned layer contained an array of through-holes to vertically aggregate the FNDs on the substrate. The through-holes were designed to have an array of 10- μm -sized FND clusters with a pitch of 20 μm . These dimensions were determined to measure the temperature distribution of mm-scaled cultured cells, such as spheroids [29], on the PDMS substrates with an appropriate spatial resolution for each cell level (typical single cell size: 10–50 μm). The patterned layer was fabricated using a resist mold containing arrayed-pillar structures with a diameter, height, and pitch of 7.8 ± 0.1 , 38.3 ± 0.2 , and 20.1 μm , respectively (Fig. S1). The channel layer had a 4-mm-wide conduit to supply the FND suspension to the through-holes. Moreover, it was designed to be ~ 150 μm tall to prevent sticking of the top surface and surface of the patterned layer and to minimize the amount of FND suspensions used in assembly. The fabricated template had a patterned layer that was 39.0 ± 0.2 μm thick, along with through-holes having a diameter of 8.6 ± 0.2 μm , arrayed at a pitch of 20.2 ± 0.1 μm (Fig. 3(a, b, and c)). The through-holes were not perfectly cylindrical, and their diameters widened up to ~ 13 μm near the top and bottom (Fig. 3(c)) due to the shape of the resist mold (Fig. S1).

4.2. Fabrication of FND clusters

Clusters were fabricated using FNDs with average sizes of 70, 140, and 750 nm (Fig. S2(a) and (b)). The concentration of the suspension was varied to demonstrate that the assembly process permitted vertical aggregation of FNDs on the substrate. Herein, each experimental condition is described as “FND size (suspension concentration);” for example “70 nm (1.0%)” indicates that the fabrication was conducted using 70 nm FNDs at a suspension concentration of 1.0% w/v.

Following assembly with the fabricated template, the FNDs were assembled on the substrate with a 30 μm thick PDMS layer (Fig. 4(a and b), and S2(c)). The obtained images confirmed that the FNDs aggregated

on the target substrates and the FND clusters were arrayed over an area of 1 mm^2 . The cluster diameter at the substrate surface prepared using 70, 140, and 750 nm FNDs was 12.7 ± 0.8 , 12.3 ± 0.8 , and 10.2 ± 0.6 μm , respectively. The clusters with smaller FNDs had larger diameters because the smaller FNDs deeply penetrated the gap between the template and the substrate at the edge of the through-holes, and this finding was consistent for different suspension concentrations (Fig. 3(c)). The shape and volume of the clusters were then quantitatively evaluated by capturing 3D profiles of 60 randomly selected FND clusters under each fabrication condition using a laser scanning microscope (Fig. 4(c) and S2(d)). The height profiles indicated that the height of the clusters increased with increasing suspension concentration across all FND sizes. Clusters with 70 and 140 nm FNDs showed similar profiles, with recessed areas near the center and more FNDs located in the outer region of the clusters. For 70 nm (4.0%) and 140 nm (4.0%), the height of the cluster at a location 3.9 μm away from the center of the cluster was 0.9 ± 0.1 μm and 1.3 ± 0.2 μm , respectively; these values correspond to ten FNDs, indicating that the FNDs aggregated vertically on the substrate. By contrast, the profiles of the 750 nm clusters (0.25, 0.5, and 1.0%) showed that the FNDs aggregated vertically and the height of the clusters tended to be higher at the center. However, a significant variation in height ($\sim 30\%$) was observed at every position.

The apparent volume of each cluster was estimated based on the height profiles. Notably, this estimation did not consider the gaps between the FNDs because the laser microscope scanned only the surface of the clusters. The average volume of the clusters increased with increasing suspension concentration across all FND sizes (Fig. 4(d) and Table 1). Moreover, the volume of the clusters obtained from the 750 nm FNDs varied significantly (over $\pm 30\%$) across different suspension concentrations, similar to the height profile results. By contrast, less variation was observed in the volume of the clusters obtained from 70 and 140 nm FNDs, particularly when using the 4.0% w/v suspension (Table 1). Subsequently, the number of FNDs in the clusters was estimated by simply dividing the volume of the clusters by the cube of the average FND size, which indicated that $1.8 \times 10^5 \pm 1.8 \times 10^4$, $2.8 \times 10^4 \pm 2.7 \times 10^3$, and $2.6 \times 10^2 \pm 1.3 \times 10^2$ FNDs were present in the clusters obtained from 70 nm (4.0%), 140 nm (4.0%), and 750 nm (1.0%), respectively.

The microfluidics-guided assembly was also applied to other substrate materials including Si, glass, Al_2O_3 , and a collagen vitrigel membrane. The results of these substrate materials using 140 nm FNDs were similar to those the PDMS substrate (Fig. S2(e)), indicating the applicability of the proposed process to various substrate materials.

4.3. Evaluation of FND clusters for thermometry

To demonstrate that the vertical aggregation of FNDs helped achieve enhanced sensitivity, the fluorescence spectra of the clusters were acquired using an epifluorescence microscope (Fig. 5(a)). Each FND cluster was independently excited using a 594 nm laser, and its fluorescence spectrum was recorded for 20 s. The fabricated clusters

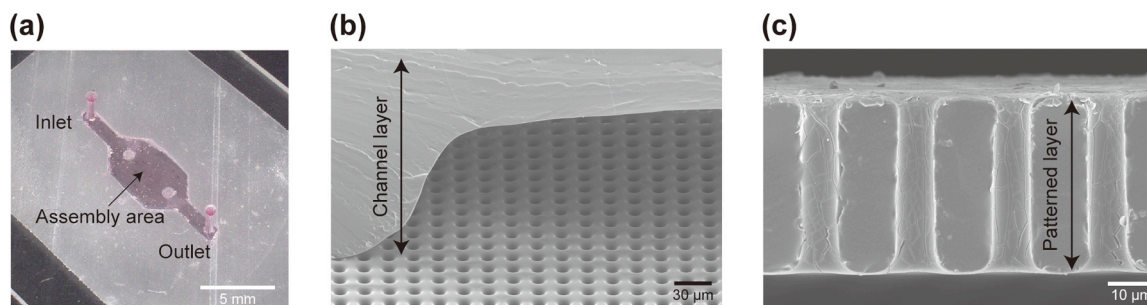


Fig. 3. PDMS-based microfluidic template for FND assembly. **a** Entire structure of the PDMS microfluidic template. **b** SEM image of channel layer with through-holes. **c** SEM image of through-holes in patterned layer in cross-sectional view.

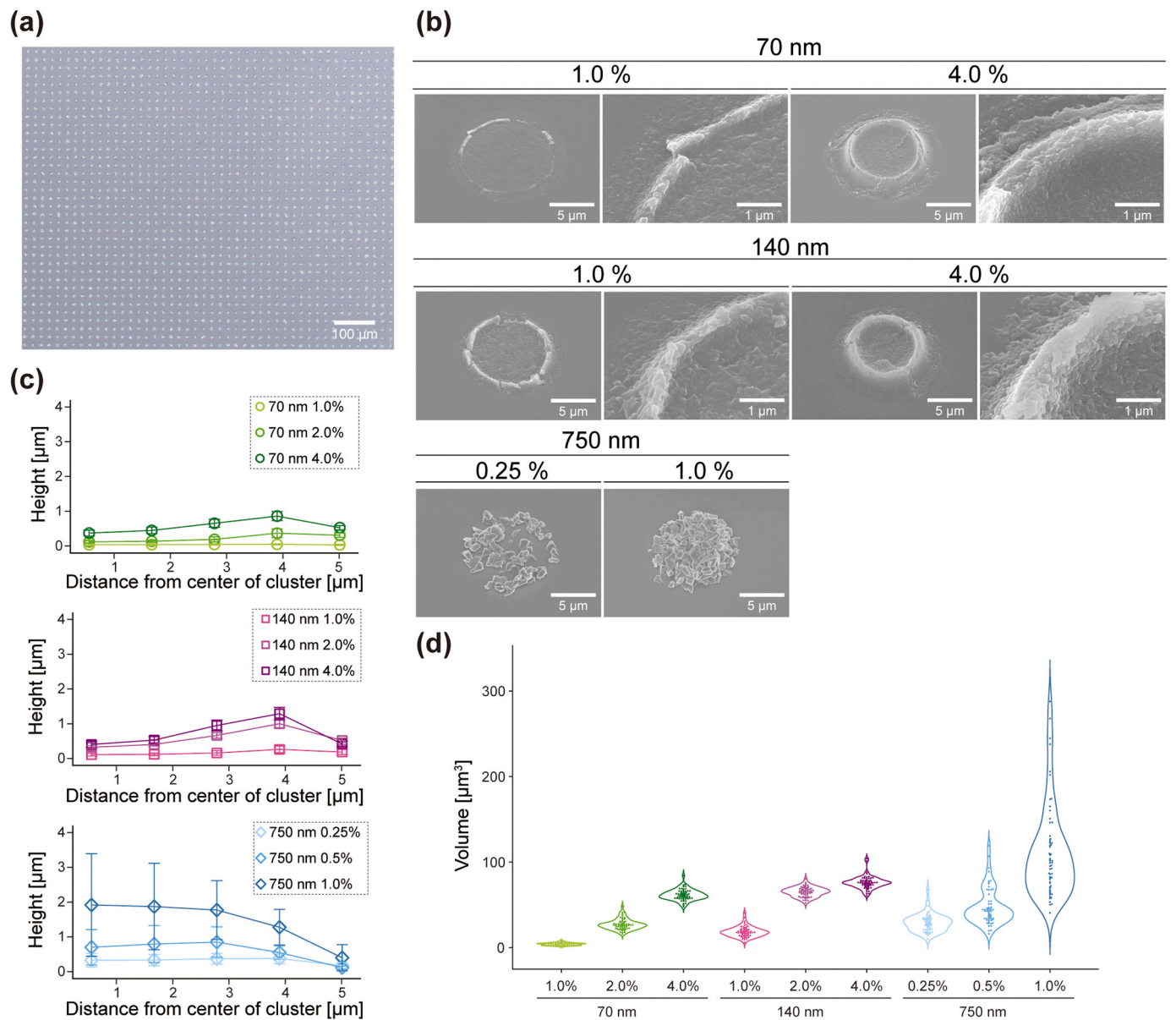


Fig. 4. Evaluation of fabricated FND clusters. **a** Optical micrograph of arrayed FND clusters on a PDMS-coated glass substrate. **b** SEM images of FND clusters containing 70, 140, and 750 nm FNDs at different concentrations. **c** Height profiles of the fabricated FND clusters. Each cluster was divided into five zones with respect to the center. **d** Violin plot of estimated volume for the fabricated FND clusters, with each condition corresponding to 60 clusters.

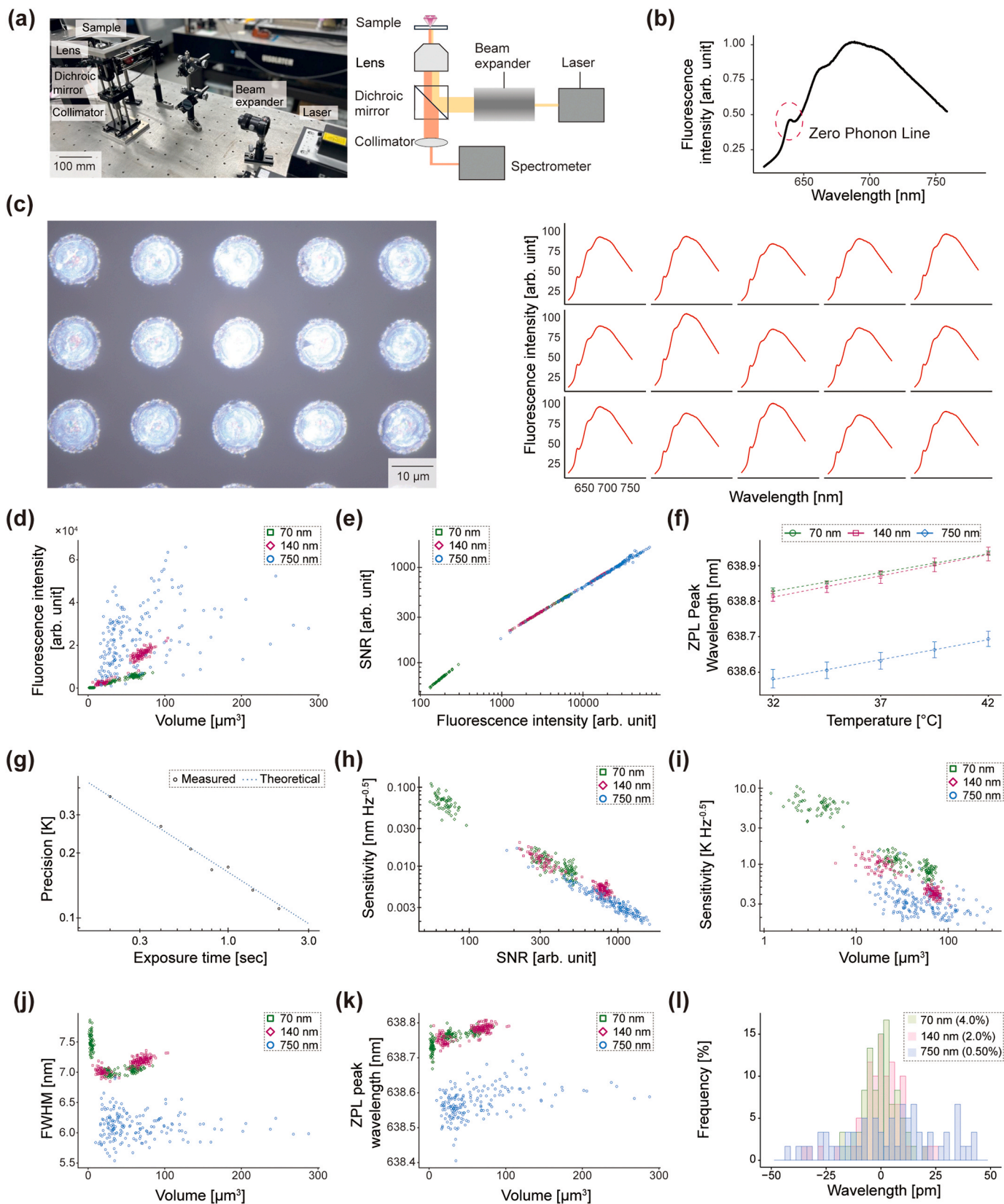
Table 1
Estimated volume of FND clusters.

FND size	70 nm			140 nm			750 nm		
Concentration	1.0 %	2.0 %	4.0 %	1.0 %	2.0 %	4.0 %	0.25 %	0.50 %	1.0 %
Volume [μm ³]	4 ± 2	27 ± 6	62 ± 6	18 ± 6	65 ± 6	76 ± 7	29 ± 10	47 ± 21	111 ± 54

exhibited fluorescence of NVCs with the zero-phonon line (ZPL) appearing as a peak at ~638 nm under ambient conditions (23 °C), whose spectrum shape depends on temperature[7] (Fig. 5(b) and (c)). First, the fluorescence intensity of the FND clusters was investigated, given its influence on sensitivity. The fluorescence intensity of the clusters was assumed to increase with increasing volume because the fluorescence of each FND was superimposed. Therefore, the fluorescence intensity was plotted against the volume (Fig. 5(d)), and the results showed that the fluorescence intensity increased with increasing cluster volume across all FND sizes. The coefficient of determination (R^2

value) of the linear fit for the fluorescence intensity–cluster volume plots was 0.98, 0.97, and 0.38 for the clusters with 70, 140, and 750 nm FNDs, respectively, with the slope of the plot being greater for larger FNDs. Next, the SNR of the fluorescence spectrum was investigated as a function of fluorescence intensity (Fig. 5(e)). The SNR and fluorescence intensity showed a linear relationship, regardless of the FND size, with an R^2 value of 0.9982 and slope of 0.537 in the log-log plot. These results demonstrate that increasing the cluster volume by vertically aggregating FNDs enhanced the fluorescence intensity and improved the SNR.

Next, improvements in sensitivity were investigated by analyzing the



(caption on next page)

Fig. 5. Fluorescence measurements of FND clusters. **a** Illustration and photograph of an inverted optical microscope system integrated with a spectrometer to acquire fluorescence spectra. **b** Fluorescence spectrum of assembled FND clusters containing 140 nm FNDs at 23 °C. **c** Optical image of FND clusters and the corresponding fluorescence spectra. **d** Scatter plot showing the relationship between the fluorescence intensity and volume of FND clusters. **e** Scatter plot showing the relationship between signal-to-noise ratio (SNR) and fluorescence intensity of FND clusters. **f** Shifts in zero-phonon line (ZPL) peak wavelength over 32–42 °C, with 10 FND clusters considered for determining the size of each FND, and each datapoint and error bar representing mean \pm standard deviation. **g** Scatter plot showing the relationship between integration time and precision. The dotted line represents the theoretical relationship with a slope of -0.5 . **h** Scatter plot showing the relationship between the wavelength-scale sensitivity and SNR of FND clusters. **i** Scatter plot showing the relationship between the temperature sensitivity and volume of FND clusters. **j** Scatter plot showing the relationship between FWHM of ZPL and FND cluster volume. **k** Scatter plot showing the relationship between ZPL peak wavelength and FND cluster volume. **l** Histogram showing the variance of ZPL peak wavelength from the average peak for 70 nm (4.0 %), 140 nm (2.0 %), and 750 nm (0.50 %). Each datapoint in **d**, **e**, **h**, **i**, **j**, and **k** corresponds to an individual FND cluster, with different colors indicating the various sizes of the FNDs. (180 clusters considered for each FND size).

acquired spectrum using all-optical methods[7]. To determine the ZPL peak wavelength which functioned as an indicator of temperature, a sum of the Voigt and exponential functions representing the ZPL (Lorentzian function) convolved with the instrument function (Gaussian function) and phonon side band spectra, respectively[14,19,28,30,31], (see the Materials and methods) was used as a fitting function (Fig. S3(a)). First, the viability of the FND clusters as thermometers was explored by placing them on a temperature-regulated stage and acquiring their fluorescence spectra. The ZPL spectra of clusters with 70, 140, and 750 nm FNDs shifted in the range of 32–42 °C, a temperature range relevant for biological applications, (Fig. S3(b)) with the linear thermal shift of the ZPL peak wavelength being 11 ± 1 , 12 ± 1 , and 11 ± 2 pm/K, and the corresponding R^2 value being 0.998, 0.997, and 0.997, respectively (Fig. 5(f)). Next, using sensitivity as an indicator of precision was investigated by changing the integration time and performing a comparison with the theoretical model. Theoretically, as the integration time increases by a factor of T , the noise decreases by a factor of $1/\sqrt{T}$, leading to an improvement in SNR by a factor of \sqrt{T} [32]. Because precision is inversely proportional to the SNR, the slope of the log-log plot between integration time and precision revealed the relationship between these parameters. The measured data corresponded to the theoretical line (Fig. 5(g)); therefore, the sensitivity was used to evaluate the temperature-measurement performance of the FND clusters. Finally, the sensitivity enhancement due to the improvement in SNR by the vertical aggregation of FNDs was investigated. The sensitivity of the ZPL peak wavelength was termed the wavelength sensitivity, while the sensitivity converted to a temperature scale by considering the measured ZPL peak shift was termed the temperature sensitivity. The wavelength sensitivity of each cluster correlated with the corresponding SNR (Fig. 5(h)). Wavelength sensitivity was enhanced with an increase in SNR, and the relationship between wavelength sensitivity and SNR did not depend on the FND size. The slope of the plot (-1.08) and the R^2 value (0.966) indicated that sensitivity was inversely proportional to the SNR. The improvement in sensitivity due to the vertical aggregation of FNDs was demonstrated using temperature sensitivity-cluster volume plots (Fig. 5(i)) and the fluctuation in the output temperature signal from the FND clusters (Fig. S3(c)). Because the fluorescence intensity per cluster volume was higher for larger FNDs (Fig. 5(d)), the temperature sensitivity for similar cluster volumes was also higher for larger FNDs and reached 0.27 ± 0.06 K Hz $^{-0.5}$ for 750 nm (0.50 %) (Table 2).

Finally, the changes in the cluster-specific ZPL due to vertical aggregation of the FNDs were examined. First, the sharpness of the ZPL was evaluated using the FWHM. The FWHM–volume plot of the clusters showed that the FWHM varied depending on the FND size; however, no consistent increase or decrease in the FWHM was observed relative to

the cluster volume for all FND sizes (Fig. 5(j)). Notably, variance in the ZPL peak wavelength has been reported among FNDs, even those of the same size[14], leading to inaccurate temperature measurements; therefore, the ZPL peak wavelength of each cluster was investigated. As the cluster volume increased, the ZPL was expected to become more uniform, and the variance in the ZPL peak wavelength was expected to decrease. Upon plotting the ZPL peak wavelength of the clusters against the corresponding cluster volume (Fig. 5(k)), the variance in the ZPL peak wavelength was found to decrease with increasing cluster volume across all FND sizes. Comparing the variance in the ZPL peak wavelength between the 70 nm (4.0 %), 140 nm (2.0 %), and 750 nm (0.50 %) clusters, whose average cluster volumes were similar, the variance was found to be smaller for smaller FNDs (Fig. 5(l)). The accuracy of the temperature measurement for each fabrication condition, defined by the variance in the ZPL peak wavelength, was enhanced by increasing the suspension concentration (Table 3). This finding shows that the vertical aggregation of FNDs reduces the variance of the ZPL peak wavelength, enabling accurate temperature mapping when using all-optical methods.

5. Discussion

In this study, a microfluidics-guided assembly method for FND clusters was established to enhance the sensitivity of FND-based thermometry. This approach enabled the vertical aggregation of FNDs within arrayed spots defined by a microfluidic template. Vertical aggregation resulted in an improved SNR with increased fluorescence intensity. Enhancement in sensitivity owing to SNR improvement was demonstrated using an all-optical method. Furthermore, the variance in the ZPL peak wavelength among the clusters was reduced, leading to superior temperature-mapping accuracy. In our study, the clusters comprising 750 nm FNDs displayed the highest sensitivity, while those with 70 nm FNDs exhibited the highest accuracy.

First, the height profiles of the clusters obtained via the assembly process were observed to vary with the FND size. The assemblies of 70 and 140 nm FNDs resulted in ring-like profiles, while the 750 nm FNDs tended to assemble near the center of the cluster (Fig. 4(b) and (c)). Additionally, the cluster volume depended on the FND size (Fig. 4(d)), with larger FNDs (750 nm) producing significantly bigger clusters ($111 \mu\text{m}^3$) than those obtained from smaller FNDs (70 nm ($4 \mu\text{m}^3$) and 140 nm ($18 \mu\text{m}^3$)), even at the same suspension concentration (1.0 %). These differences are attributed to the variation in the dispersion state of the FNDs in the template. Smaller FNDs (70, and 140 nm) were more evenly dispersed and carried by the flow during the drying of the suspension (Fig. S2(b) and (c)), resulting in smaller clusters with ring-like profiles caused by a coffee-ring effect. In contrast, larger FNDs (750 nm) precipitated quickly and allowed the clusters to form before

Table 2
Temperature sensitivity of FND cluster.

FND size	70 nm			140 nm			750 nm		
	Concentration	1.0 %	2.0 %	4.0 %	1.0 %	2.0 %	4.0 %	0.25 %	0.50 %
Sensitivity [K Hz $^{-0.5}$]	6.1	1.2 \pm 0.2	0.82 \pm 0.14	1.0 \pm 0.2	0.43 \pm 0.05	0.41 \pm 0.06	0.47 \pm 0.23	0.27 \pm 0.06	0.29 \pm 0.10

Table 3
Accuracy based on the variance of ZPL peak wavelength.

FND size	70 nm			140 nm			750 nm		
	Concentration	Accuracy [K]		Concentration	Accuracy [K]		Concentration	Accuracy [K]	
Concentration	1.0 %	2.0 %	4.0 %	1.0 %	2.0 %	4.0 %	0.25 %	0.50 %	1.0 %
Accuracy [K]	2.0	0.83	0.72	1.1	0.90	0.91	3.2	2.9	2.9

the suspension was completely dry (Fig. S2(b) and (c)), resulting in larger clusters without ring-like profiles. These results suggest that the behavior of FNDs in the suspension played a crucial role in determining the profile and volume of the clusters. Thus, to effectively control the cluster profile and volume, the solvent type, pH, and ion concentration—which also affect the FND behavior—should be investigated.

Next, the SNR improvements due to the vertical aggregation of the FNDs were explored. The strong positive correlation between the SNR and fluorescence intensity (Fig. 5(e)) underscored the benefits of enhancing the fluorescence intensity to improve the SNR. Thus, by focusing on the fluorescence intensity, clusters with smaller FNDs were found to exhibit weaker fluorescence intensity per cluster volume (Fig. 5(d)). This phenomenon could potentially be caused by the difference in the properties of single FNDs, such as size and shape[33,34] and the density of other impurities in FNDs[35], which have been reported as factors affecting the fluorescence intensity. However, the cause was not clarified in the present study; thus, further investigation is required to understand this phenomenon and select an appropriate FND size for realizing a high SNR.

To demonstrate an enhancement in sensitivity via an increase in the SNR improvement, the clusters were confirmed to function as thermometers with thermal shifts of the ZPL peak wavelength ranging from 11 to 12 pm/K (Fig. 5(f) and S3(b)). In previous studies, the theoretical shift estimated using the vibrational model was 13.5 pm/K at 303 K [36], whereas the experimental shift of FNDs ranged from 13 to 19 pm/K [14,30,31,37]. Although the present study yielded smaller shifts than those reported previously, this aspect can be considered a characteristic of the FNDs, given the large variation in the reported values. Regarding sensitivity, the SNR improvement was found to enhance sensitivity (Fig. 5(h) and (i)), proving the utility of the microfluidics-guided assembly, which helped increase the number of FNDs in the excitation spot by vertical aggregation. Notably, an all-optical method was used in this study to investigate the sensitivity enhancement (Table 2); however, FND clusters can also be used with spin-based methods, which result in higher sensitivity than that of all-optical methods[7].

Considering the ZPL of the fabricated FND clusters, the ZPL peak wavelength appeared at different positions depending on the FND size (Fig. 5(f) and (k)). The ZPL peak wavelength can vary for each particle because of differences in the impurity concentration, strain, and surface geometry[38]. These factors are influenced by the FND manufacturing process, which can cause the ZPL peak wavelength to vary with the FND size. For the same reason, the FWHM of the ZPL also depends on the FND size. When the effects of the FND assembly on the ZPL sharpness were analyzed using the FWHM, no consistent increase or decrease in the FWHM was observed with increasing FND cluster volume across all FND sizes (Fig. 5(k)). Therefore, in this study, neither sharpening nor broadening of the ZPL occurred owing to FND aggregation, presumably because the variance in the ZPL peak wavelength among the FNDs was sufficiently small relative to the FWHM, resulting in no clear trends. Notably, the FWHM of 70 nm (1.0 %) was higher than that of the others because the fluorescence intensity was remarkably weak (Fig. 5(h)) and the ZPL shape was affected by the background.

The variance in the ZPL peak wavelength among the FND clusters, which is important for accurate temperature mapping using all-optical methods, was also investigated. In this regard, an increase in cluster volume was found to help reduce the variance of the ZPL peak wavelength among the clusters, thereby enhancing the accuracy (Fig. 5(k)) owing to the superimposition of the ZPLs from individual FNDs, which

led to an averaged ZPL peak position. This result emphasizes the key advantage of our assembly method, that is, enabling the arrangement of FND clusters on the substrate for temperature mapping.

Our investigation of different FND sizes suggests that using larger FNDs may be beneficial for enhancing sensitivity (Table 2), while using smaller FNDs for cluster fabrication may be effective for improving accuracy (Table 3). Under our current all-optical measurement configuration, 0.9 and 90 sec were required for each cluster to achieve measurements with 1 and 0.1 K precision, respectively, when 70 nm FNDs were used for fabricating the clusters. Furthermore, the clusters array with 70 nm FNDs achieved 0.6 K accuracy. Therefore, these clusters may be used to achieve the highly accurate temperature mapping of slowly changing objects on a time scale of minutes to hours. For example, time transient temperature mapping of cultured cells on a cell culture substrate over several days may be used to evaluate their metabolism [29]. In contrast, 0.1 and 1 sec were required for each cluster to achieve measurements with 1 and 0.1 K precision when 750 nm FNDs were used. Although the accuracy of the clusters with 750 nm FNDs at approximately 3 K was worse than that of 70 nm FNDs, the time resolution may be improved. Therefore, these clusters may be applied measurements including temperature sensing during the laser processing of materials to evaluate laser heating, which generally requires sub-second time resolution [20].

Compared with previous FNDs assembly methods, our approach offers distinct advantages in vertically aggregating FNDs within defined spots of a specific size excited by a laser which effectively enhances both sensitivity and accuracy as proven by our results. Although the methods using chemical forces created by metal patterns[15,21] or functional groups[22,23] on the substrate enable the directly assembly of FNDs, these methods limit FNDs assembly to a monolayer-like form. By contrast, our microfluidics-guided assembly allows the accumulation of at minimum ten FNDs in the vertical direction (Fig. 4(c)). Furthermore, our method enables FND assembly without specific patterning on the substrate itself. 3D aggregation of FNDs can also be realized using optical tweezers as described in a previous report[19], but our approach is more practical, requiring only a soft-lithography-based process for microfluidic template fabrication. Thus, our method provides a scalable and efficient solution for achieving FND assemblies suitable for practical applications in highly sensitive and accurate temperature mapping and its time transient.

Our microfluidics-guided assembly realizes the collective fabrication of FND clusters that function as sensitive, accurate thermometers. The FND cluster array can be applied for real-time temperature mapping with sub-kelvin-level sensitivity and accuracy (Tables 2 and 3). To extend our approach to assemble FNDs within small spots and pitches for high-resolution mapping, the dimensions of the through-holes should be reduced. Various methods have been used to fabricate PDMS layers with sub-micrometer-diameter through-holes, such as using other materials as a mold[39] or directly making through-holes by dry etching[40]. For example, < 1- μ m-diameter Si pillars with an aspect ratio of 20 have been fabricated by deep reactive ion etching[41]. By combining these technologies, our method could achieve spatial resolutions of up to 1 μ m, enabling highly sensitive, accurate, and high-resolution temperature mapping, accelerating research in chemistry, electronics, and biology.

6. Conclusion

A microfluidics-guided assembly method was devised to improve the sensitivity of FND-based thermometry. A PDMS microfluidic template

featuring an array of through-holes enabled the direct, collective, and vertical aggregation of FNDs on the target substrate. Owing to vertical aggregation, the SNR of the fluorescence was enhanced with increasing fluorescence intensity. Additionally, this SNR improvement led to an enhancement in sensitivity. Moreover, the variance in the ZPL peak wavelength was reduced, enhancing the accuracy. The template was fabricated using a soft-lithography-based process, thereby providing a practical approach for highly sensitive, accurate FND-based thermometry in applications including temperature mapping. Furthermore, our assembly approach does not rely on the NP–substrate interactions, making it widely applicable to various combinations of NPs and substrates. Therefore, the microfluidics-guided assembly scheme may contribute not only to fluorescence-based sensing, but also to other applications rooted in nanoparticle technologies, such as displays[42] and encryption[43].

CRediT authorship contribution statement

Zetsu Masaya: Investigation. **Saikawa Keita:** Writing – original draft, Investigation, Formal analysis, Data curation, Conceptualization. **Shikama Taiichi:** Writing – review & editing, Visualization, Validation, Methodology, Investigation, Formal analysis, Data curation. **Ueshima Daiki:** Investigation, Data curation. **Kamei Ken-ichiro:** Writing – review & editing, Visualization, Validation, Supervision. **Hirai Yoshikazu:** Writing – review & editing, Visualization, Validation, Supervision, Resources, Project administration, Methodology, Investigation, Funding acquisition, Conceptualization. **Tabata Osamu:** Writing – review & editing, Validation, Project administration, Funding acquisition.

Declaration of Competing Interest

Osamu Tabata is an Editor for the journal, no other author has reported any competing interest.

Acknowledgments

This research was supported by JSPS KAKENHI (grant no. JP23H00260) and the Advanced Research Infrastructure for Materials and Nanotechnology in Japan (ARIM)" of the Ministry of Education, Culture, Sports, Science and Technology (MEXT). Proposal Number JPMX1224KT2232. We thank Mr. Kosuke Ishikawa at the Department of Mechanical Engineering and Science, Kyoto University, for conducting the SEM observations for this study and Editage's support for providing English language editing assistance for this manuscript.

Author contributions

K.S. and Y.H. conceptualized the study. K.S., Y.H., and K.K. planned the experiments. K.S., M.Z., D.U., and T.S. conducted the experiments. K.S., T.S., K.K., and Y.H. performed data analysis. All the authors contributed to the discussion and interpretation of this manuscript. K.S. wrote the initial draft of the manuscript. Y.H., K.K., T.S., and O.T. reviewed and edited the manuscript.

Appendix A. Supporting information

Supplementary data associated with this article can be found in the online version at [doi:10.1016/j.sna.2025.116312](https://doi.org/10.1016/j.sna.2025.116312).

Data availability

Data will be made available on request.

References

- [1] M. Fujiwara, Diamond quantum sensors in microfluidics technology, *Biomicrofluidics* 17 (2023) 054107.
- [2] T.F. Segawa, R. Igarashi, Nanoscale quantum sensing with nitrogen-vacancy centers in nanodiamonds – A magnetic resonance perspective, *Prog. Nucl. Magn. Reson. Spectrosc.* 134–135 (2023) 20–38.
- [3] K.O. Ho, et al., Diamond quantum sensors: from physics to applications on condensed matter research, *Funct. Diam.* 1 (2021) 160–173.
- [4] S. Hong, et al., Nanoscale magnetometry with NV centers in diamond, *MRS Bull.* 38 (2013) 155–161.
- [5] F. Dolde, et al., Electric-field sensing using single diamond spins, *Nat. Phys.* 7 (2011) 459–463.
- [6] G.-Q. Liu, R.-B. Liu, Q. Li, Nanothermometry with enhanced sensitivity and enlarged working range using diamond sensors, *Acc. Chem. Res.* 56 (2023) 95–105.
- [7] M. Fujiwara, Y. Shikano, Diamond quantum thermometry: from foundations to applications, *Nanotechnology* 32 (2021) 482002.
- [8] T. Fujisaku, et al., pH nanosensor using electronic spins in diamond, *ACS Nano* 13 (2019) 11726–11732.
- [9] R. Tanos, et al., Optimal architecture for diamond-based wide-field thermal imaging, *AIP Adv.* 10 (2020) 025027.
- [10] S.-J. Yu, M.-W. Kang, H.-C. Chang, K.-M. Chen, Y.-C. Yu, Bright fluorescent nanodiamonds: no photobleaching and low cytotoxicity, *J. Am. Chem. Soc.* 127 (2005) 17604–17605.
- [11] M. Quintanilla, L.M. Liz-Marzan, Guiding rules for selecting a nanothermometer, *Nano Today* 19 (2018) 126–145.
- [12] G.-Q. Liu, X. Feng, N. Wang, Q. Li, R.-B. Liu, Coherent quantum control of nitrogen-vacancy center spins near 1000 kelvin, *Nat. Commun.* 10 (2019) 1344.
- [13] M. Fukami, et al., All-optical cryogenic thermometry based on nitrogen-vacancy centers in nanodiamonds, *Phys. Rev. Appl.* 12 (2019) 014042.
- [14] Y.Y. Hui, et al., All-optical thermometry with nitrogen-vacancy centers in nanodiamond-embedded polymer films, *J. Phys. Chem. C* 123 (2019) 15366–15374.
- [15] P. Andrich, et al., Microscale-resolution thermal mapping using a flexible platform of patterned quantum sensors, *Nano Lett.* 18 (2018) 4684–4690.
- [16] A.M. Schrand, et al., Are diamond nanoparticles cytotoxic? *J. Phys. Chem. B* 111 (2007) 2–7.
- [17] K.-K. Liu, C.-L. Cheng, C.-C. Chang, J.-I. Chao, Biocompatible and detectable carboxylated nanodiamond on human cell, *Nanotechnology* 18 (2007) 325102.
- [18] G. Reina, L. Zhao, A. Bianco, N. Komatsu, Chemical functionalization of nanodiamonds: opportunities and challenges ahead, *Angew. Chem. Int. Ed.* 58 (2019) 17918–17929.
- [19] T. Wu, et al., Intracellular thermal probing using aggregated fluorescent nanodiamonds, *Adv. Sci.* 9 (2022) 2103354.
- [20] Y.-K. Tzeng, et al., Time-resolved luminescence nanothermometry with nitrogen-vacancy centers in nanodiamonds, *Nano Lett.* 15 (2015) 3945–3952.
- [21] M. Jiang, J.A. Kurvits, Y. Lu, A.V. Nurmikko, R. Zia, Reusable inorganic templates for electrostatic self-assembly of individual quantum dots, nanodiamonds, and lanthanide-doped nanoparticles, *Nano Lett.* 15 (2015) 5010–5016.
- [22] S.G. Rao, et al., Directed assembly of nanodiamond nitrogen-vacancy centers on a chemically modified patterned surface, *ACS Appl. Mater. Interfaces* 6 (2014) 12893–12900.
- [23] M. Kianinia, et al., Robust, directed assembly of fluorescent nanodiamonds, *Nanoscale* 8 (2016) 18032–18037.
- [24] I.K. Dimov, et al., Stand-alone self-powered integrated microfluidic blood analysis system (SIMBAS), *Lab Chip* 11 (2011) 845–850.
- [25] C. Hamon, et al., Tunable nanoparticle and cell assembly using combined self-powered microfluidics and microcontact printing, *Adv. Funct. Mater.* 26 (2016) 8053–8061.
- [26] Y. Hirai, et al., ALA-induced fluorescence detection with photoresist-based microfluidic cell sorter for bladder cancer diagnosis, *Sens. Actuators B* 213 (2015) 547–557.
- [27] Y. Hirai, Y. Inamoto, K. Sugano, T. Tsuchiya, O. Tabata, Moving mask UV lithography for three-dimensional structuring, *J. Micromech. Microeng.* 17 (2006) 199.
- [28] T. Plakhotnik, H. Aman, H.-C. Chang, All-optical single-nanoparticle radiometric thermometry with a noise floor of $0.3 \text{ K Hz}^{-1/2}$, *Nanotechnology* 26 (2015) 245501.
- [29] A. Kumar, V.S. Goudar, K. Kaladharan, T.S. Santra, F.-G. Tseng, Synthesis and characterization of a fluorescent polymeric nano-thermometer: dynamic monitoring of 3D temperature distribution in co-cultured tumor spheroids, *Analyst* 148 (2023) 2045–2057.
- [30] P.-C. Tsai, et al., Measuring nanoscale thermostability of cell membranes with single gold–diamond nanohybrids, *Angew. Chem.* 129 (2017) 3071–3076.
- [31] T. Shikama, T. Watanabe, M. Jouda, M. Hasuo, A tesla-order magnetic field effect on all-optical thermometry using photoluminescence spectrum of diamond NV⁻ center, *Jpn. J. Appl. Phys.* 60 (2020) 012001.
- [32] M. Gupta, et al., Cross-correlated quantum thermometry using diamond containing dual-defect centers, *Adv. Sens. Res.* 3 (2024) 2300103.
- [33] M.D. Torelli, N.A. Nunn, O.A. Shenderova, A perspective on fluorescent nanodiamond bioimaging, *Small* 15 (2019) 1902151.
- [34] H. Wen, et al., Correlative fluorescence and transmission electron microscopy assisted by 3D machine learning reveals thin nanodiamonds fluoresce brighter, *ACS Nano* 17 (2023) 16491–16500.

- [35] L.-J. Su, et al., Creation of high density ensembles of nitrogen-vacancy centers in nitrogen-rich type Ib nanodiamonds, *Nanotechnology* 24 (2013) 315702.
- [36] M.W. Doherty, et al., Temperature shifts of the resonances of the NV⁻ center in diamond, *Phys. Rev. B* 90 (2014) 041201.
- [37] L. Ishikawa, et al., All-optical thermometry using a single multimode fiber endoscope and diamond nanoparticles containing nitrogen vacancy centers, *Rev. Sci. Instrum.* 93 (2022) 083705.
- [38] C. Foy, et al., Wide-field magnetic field and temperature imaging using nanoscale quantum sensors, *ACS Appl. Mater. Interfaces* 12 (2020) 26525–26533.
- [39] Y.-H. Nam, S.-K. Lee, J.-H. Kim, J.-H. Park, PDMS membrane filter with nano-slit array fabricated using three-dimensional silicon mold for the concentration of particles with bacterial size range, *Microelectron. Eng.* 215 (2019) 111008.
- [40] W.F. Quiros-Solano, et al., Microfabricated tuneable and transferable porous PDMS membranes for Organs-on-Chips, *Sci. Rep.* 8 (2018) 13524.
- [41] Y.-F. Chang, Q.-R. Chou, J.-Y. Lin, C.-H. Lee, Fabrication of high-aspect-ratio silicon nanopillar arrays with the conventional reactive ion etching technique, *Appl. Phys. A* 86 (2007) 193–196.
- [42] T. Meng, et al., Ultrahigh-resolution quantum-dot light-emitting diodes, *Nat. Photonics* 16 (2022) 297–303.
- [43] D. Guo, et al., Embossed template induced particles assembly for heterostructures and the application in high-security encryption, *Adv. Funct. Mater.* 33 (2023) 2210952.

Keita Saikawa is a research assistant in the Department of Mechanical Engineering and Science, Kyoto University, Japan. He obtained his Master's degree in Engineering from Kyoto University. His research is in development of sensors for organs-on-a-chip technologies.

Masaya Zetsu received his B.E. degree in Engineering Science and M.E. degree in Mechanical Engineering and Science from Kyoto University in 2022 and 2024, respectively. He is currently a member of DISCO Corp.

Daiki Ueshima received his B.E. degree in Engineering Science from Kyoto University in 2024. He is currently a master's student in the Department of Mechanical Engineering and Science at Kyoto University.

Taiichi Shikama received his B.E. degree in Systems Innovation and M.E. degree and Ph. D. in Quantum Engineering and Systems Science from the University of Tokyo in 2002,

2004, and 2007, respectively. He is currently an associate professor in the Department of Mechanical Engineering and Science at Kyoto University.

Ken-ichiro Kamei is an Associate Professor with joint appointments in Biology and Bioengineering at NYU Abu Dhabi and a visiting associate professor at Kyoto University's iCeMS. He earned his BA (1998), MS (2000), and PhD (2003) from the Tokyo Institute of Technology. His research focuses on creating the "Body on a Chip" device to replicate physiological and pathological conditions in vitro. By integrating stem cell biology, chemical biology, and micro/nanotechnology, he advances regenerative medicine and drug discovery for humans and endangered animals. He is an Editor-in-Chief of *Cell Engineering Connect*, and an Editorial Board Member of *Communications Biology*.

Osamu Tabata received his M.S. degree and Ph.D. from Nagoya Institute of Technology, Japan, in 1981 and 1993, respectively. In 1981, he joined the Toyota Central Research and Development Laboratories, Inc., Japan. In 1996, he joined the Department of Mechanical Engineering, Ritsumeikan University, Japan. In 2003, he moved to the Graduate School of Engineering, Kyoto University. In October 2019, he moved to the Kyoto University of Advanced Science as a founding Dean of the Faculty of Engineering and Graduate School of Engineering. From December 2022, he has been served as the Executive Vice President. His research is on micro/nano processes, MEMS, DNA nanotechnology. IEEE Life Fellow and IEEJ Fellow. received M.S. and Ph.D. degrees from Nagoya Institute of Technology, in 1981 and 1993, respectively. In 1981 he joined the Toyota Central Research and Development Laboratories. In 1996, he joined the Department of Mechanical Engineering at Ritsumeikan University. In 2003, he moved to the Graduate School of Engineering, Kyoto University. In October 2019, he moved to Kyoto University of Advanced Science as a founding Dean of the Faculty of Engineering and Graduate School of Engineering. From December 2022, he has been served as the Executive Vice President. His research is on micro/nano processes, MEMS, and DNA Nanotechnology. IEEE Life Fellow and IEEJ Fe.

Yoshikazu Hirai received his Ph.D. from Kyoto University, Japan, in 2007. He was an Assistant Professor with the Department of Micro Engineering, Kyoto University, in 2013. Since 2021, he has been a Junior Associate Professor with the Department of Mechanical Engineering and Science, Kyoto University. His research interests include fabrication and packaging for generic MEMS/NEMS, silicon/polymer-based MEMS devices and systems, atomic MEMS devices, and micro/nanofluidic systems for microphysiological systems. He is an Associate Editor of *IEEE Transactions on Nanotechnology*, Editorial Board Member of *Sensors and Actuators Reports* and *Cell Engineering Connect*, and a MEMS Technical Committee Member of IEEE Electron Devices Society (EDS).